Journal of Vacuum Science and Technology A

RESEARCH ARTICLE | NOVEMBER 27 2023

Al_2O_3 atomic layer deposition on a porous matrix of carbon fibers (FiberForm) for oxidation resistance

Special Collection: Atomic Layer Deposition (ALD)

Jack T. Widmer ; Steven M. George

Check for updates

J. Vac. Sci. Technol. A 41, 062412 (2023)
https://doi.org/10.1116/6.0003085

View Online
Export Citation

Articles You May Be Interested In

Atmospheric pressure plasma enhanced spatial ALD of silver

J. Vac. Sci. Technol. A (December 2014)

Understanding the effect of nitrogen plasma exposure on plasma assisted atomic layer epitaxy of InN monitored by real time grazing incidence small angle x-ray scattering

J. Vac. Sci. Technol. A (January 2019)

On the kinetics of spatial atomic layer deposition

J. Vac. Sci. Technol. A (October 2012)

14 October 2024 23:23:38



JVST A
Journal of Vacuum Science & Technology A

ARTICLE

pubs.aip.org/avs/jva

Al_2O_3 atomic layer deposition on a porous matrix of carbon fibers (FiberForm) for oxidation resistance

Cite as: J. Vac. Sci. Technol. A 41, 062412 (2023); doi: 10.1116/6.0003085
Submitted: 22 August 2023 · Accepted: 23 October 2023 ·
Published Online: 27 November 2023

View Online Export Citation CrossMark

Jack T. Widmer and Steven M. George[a)]

AFFILIATIONS

Department of Chemistry, University of Colorado, Boulder, Colorado 80309

Note: This paper is part of the 2024 Special Topic Collection on Atomic Layer Deposition (ALD).
[a)]**Electronic mail:** steven.george@colorado.edu

ABSTRACT

Atomic layer deposition (ALD) was used to coat a porous matrix of carbon fibers known as FiberForm with Al_2O_3 to improve oxidation resistance. Static trimethylaluminum (TMA) and H_2O exposures for Al_2O_3 ALD were used to obtain the uniform coating of this high porosity material. The carbon surfaces were initially functionalized for Al_2O_3 ALD by exposure to sequential exposures of nitrogen dioxide and TMA. A gravimetric model was developed to predict the mass gain per cycle under conditions when the ALD reactions reached saturation during each reactant exposure. The uniformity of the Al_2O_3 ALD coating on FiberForm was confirmed by scanning electron microscopy (SEM) and energy dispersive x-ray spectroscopy (EDS) analysis. The SEM, EDS, and gravimetric models were all consistent with a uniform Al_2O_3 ALD coating on the porous carbon fiber network when the ALD reactions reached saturation on the entire surface area. In contrast, the profile of the Al_2O_3 ALD coating on the FiberForm was also characterized using undersaturation conditions when the ALD reactions did not reach saturation throughout the FiberForm sample. Based on comparisons with results from models for ALD in porous substrates, these Al_2O_3 coverage profiles were consistent with diffusion-limited Al_2O_3 ALD. Oxidation of the FiberForm and the Al_2O_3 ALD-coated FiberForm was also investigated by thermogravimetric analysis (TGA). TGA revealed that a 50 nm thick Al_2O_3 coating deposited using 400 Al_2O_3 ALD cycles enhanced the oxidation resistance. The Al_2O_3 ALD coating increased the oxidation onset temperature by ~200 °C from 500 to 700 °C. The oxidation of the FiberForm removed carbon and left the Al_2O_3 ALD coating behind as a white "skeleton" that preserved the shape of the original FiberForm sample. The Al_2O_3 ALD coating also decreased the oxidation rate of the FiberForm by ~30%. The oxidation rate of the Al_2O_3 ALD-coated FiberForm samples was constant and independent of the thickness of the Al_2O_3 ALD coating. This behavior suggested that the oxidation is dependent on the competing O_2 diffusion into the FiberForm and CO_2 diffusion out of the FiberForm.

Published under an exclusive license by the AVS. https://doi.org/10.1116/6.0003085

14 October 2024 23:23:38

I. INTRODUCTION

Thermal protection is required to protect spacecraft from the harsh environment that vehicles encounter during atmospheric entry. The temperature at the outer surface of the spacecraft can be as high as 3000 K during atmospheric entry.[1] Single-use missions, such as the 2021 Mars Perseverance mission by the National Aeronautics Space Administration (NASA), make use of a lightweight ablative thermal protection system (TPS). Ablative TPS materials are designed to pyrolyze during re-entry.[2–4] Blocks of ablative TPS are layered on the outer surface of the spacecraft. This ablative TBS protects the underlying material by absorbing thermal energy via the pyrolysis phase change. Thermal energy is removed as the evolved gases leave the spacecraft.[2,5,6]

Carbon fiber composites have been used for thermal protection for over half a century.[7] These carbon composites can maintain their mechanical properties at very high temperatures in inert atmospheres.[8,9] Carbon is also extremely susceptible to oxidation in the presence of oxygen. Consequently, oxidation barriers are needed for carbon fiber composites to perform in oxygen environments.[10] Uncoated carbon fibers can begin to oxidize at temperatures as low as 300 °C.[11] Other studies report slightly higher

Published under an exclusive license by the AVS

oxidation threshold temperatures of 400[12] or 500 °C.[8,9,13] One ablative TPS carbon fiber composite is known as the phenolic-impregnated carbon ablator (PICA). PICA consists of a porous carbon fiber matrix called FiberForm that has been filled with a phenolic resin.[3]

Atmospheric entry to planets with dense or corrosive atmospheres will require TPS carbon fiber composite materials that are able to withstand higher thermal loads and harsh oxidative environments. Carbon fiber composite materials covered with an inorganic barrier coating could provide enhanced oxidation resistance. One method that could deposit a uniform inorganic coating on porous carbon fiber composite is atomic layer deposition (ALD). ALD is a chemical vapor deposition (CVD) process based on sequential self-limiting gas-solid reactions.[14] The self-limiting surface reactions deposit extremely conformal, uniform, and pinhole-free films. In addition, ALD can be performed at low temperatures <100 °C, if necessary to avoid damaging thermally sensitive material.[15]

Al_2O_3 ALD films are known to form excellent gas diffusion barriers.[16–19] Al_2O_3 ALD films have been used as barrier coatings for packaging materials.[20,21] Al_2O_3 ALD films have been demonstrated to improve the resistance of polymers to erosion by atomic oxygen.[22] Al_2O_3 ALD coatings also increase the oxidation temperature of Fe powders.[23] In addition, Al_2O_3 ALD films have served as oxidation barriers on carbon fibers.[11,24] A 30 nm thick coating of Al_2O_3 was shown to increase the oxidation temperature of the carbon fibers to 600 °C. A 120 nm thick Al_2O_3 ALD coating further increased the oxidation temperature of the carbon fibers to 660 °C.[11] A multilayer coating consisting of 30 nm of Al_2O_3 on top of 20 nm of TiO_2 provided an additional improvement of the oxidation onset temperature to 750 °C.[24]

ALD is uniquely suited to uniformly and conformally coat porous three-dimensional structures.[25] Al_2O_3 ALD has previously been shown to provide excellent conformal deposition on anodic aluminum oxide (AAO) membranes with high-aspect ratios.[26] ALD has also been used to uniformly coat porous and high-aspect ratio materials used in lithium-ion batteries,[27] as well as fuel cells and catalysis.[28–30] ALD should be ideal for coating the high surface area porous matrix of carbon fibers in the FiberForm.

Uniform and conformal coatings are possible because the gaseous precursors employed during ALD can diffuse through the porous network and react with the surface sites.[25,26,28,31–33] In contrast, film growth occurs preferentially on the outer surfaces of the material during chemical vapor deposition (CVD) or physical vapor deposition (PVD). Coating the outer surfaces of a porous material would then limit the ability of the reactants to reach the surface area inside the porous material. The self-limiting nature of the ALD surface reactions also ensures that the film thickness is uniform throughout the entirety of the substrate.[14,25,26,28,31]

In this work, Al_2O_3 ALD was employed to deposit Al_2O_3 barrier coatings on the FiberForm. A gravimetric model was developed to predict the mass gain per cycle under reaction conditions when the Al_2O_3 ALD reactions reached saturation during every reactant exposure. To confirm Al_2O_3 ALD on the porous carbon network, scanning electron microscopy (SEM) and energy dispersive x-ray spectroscopy (EDS) analysis were also employed to profile the Al_2O_3 ALD coating versus the number of Al_2O_3 ALD cycles. These SEM and EDS studies as well as the gravimetric model were all consistent with a uniform Al_2O_3 ALD coating on the porous carbon fiber network when the ALD reactions were in saturation. Thermogravimetric analysis (TGA) also showed that the uniform Al_2O_3 ALD coating on the FiberForm increased the threshold temperature for oxidation and lowered the oxidation rate.

II. EXPERIMENT

A. Fiberform samples and Al_2O_3 ALD reaction conditions

The initial FiberForm samples were provided by NASA Ames Laboratory. This material consists of ~10 μm carbon fibers bound into a porous matrix to form a low density solid. The fibers are arranged isotropically as observed in the secondary electron microscopy (SEM) image shown in Fig. 1. The approximate distance between the carbon fibers was 20 μm. The porosity of the FiberForm sample was ~90%. The FiberForm samples were cut into cylindrical samples that were ~1 cm in radius and ~2.5 cm tall, with a mass of ~1.3 g.

ALD was performed in a hot wall reactor as described previously.[34] Al_2O_3 ALD was conducted at a temperature of 200 °C where Al_2O_3 ALD is near its highest thickness gain per ALD cycle.[35] FiberForm substrates were placed one at a time in the reactor along with a silicon witness wafer. The FiberForm substrate was suspended between two set screws to minimize contact with the sample holder. Base pressure in the reactor under vacuum with pumping by a dual-stage rotary vane pump (Pfeiffer Vacuum, Pascal 2010 C1) was ~30 mTorr.

Trimethyl aluminum (TMA) (97%, Sigma-Aldrich) and water (H_2O) (Water ChomAR, Macron Fine Chemicals) were used as the reactants for Al_2O_3 ALD. TMA and H_2O react to form Al_2O_3 ALD

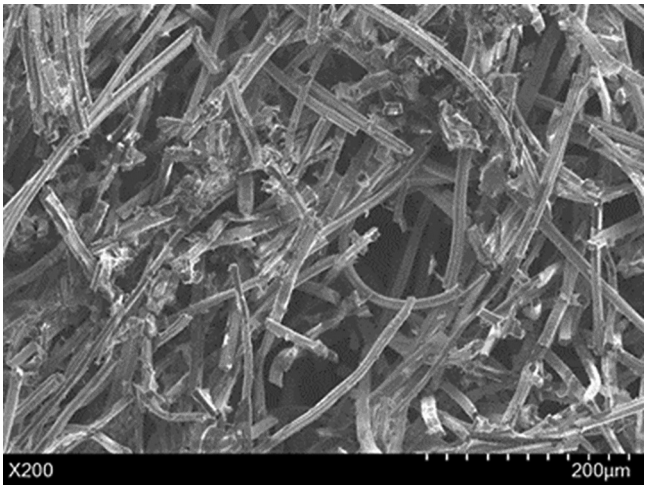


FIG. 1. Scanning electron microscopy (SEM) image of the initial FiberForm sample.

14 October 2024 23:23:38

Published under an exclusive license by the AVS

in separate reactions as follows:[35,36]

$$(\mathbf{A})\ Al-OH^{*}+Al(CH_3)_3 \rightarrow Al-O-Al(CH_3)_2^{*}+CH_4,$$

$$(\mathbf{B})\ Al-CH_3^{*}+H_2O \rightarrow Al-OH^{*}+CH_4,$$

where the asterisks identify the surface species. Monte Carlo modeling was performed to estimate the reactant exposure times and pressures needed for the TMA and H_2O reactions to reach saturation on the entire surface area of the FiberForm sample.[26]

For these estimations, the substrate was simplified by assuming parallel fibers with a length of ~1 cm along the radius of the FiberForm sample a diameter of 10 μm, and a center-to-center distance of 30 μm. This arrangement of pores is consistent with an aspect ratio of ~500. Modeling suggested that a minimum exposure time of ~1.5 s should be sufficient for the saturation of the surface reactions.[26] Given the additional tortuosity of the isotropic arrangement of the carbon fibers as illustrated in Fig. 1, the exposure durations were extended to 12 s.

Static exposures were employed for efficient precursor utilization to penetrate the porous structure of the FiberForm and coat the individual fibers. Static ALD experiments employed a timing sequence expressed as t_1–t_2–t_3–t_4–t_5–t_6. This sequence describes the duration in seconds of the dose A hold (t_1), purge (t_2), pump-down after half-cycle A (t_3), dose B hold (t_4), purge (t_5), and pump-down after half-cycle B (t_6). The dose hold is the time for the precursor dose in the chamber containing the substrate. The purge is conducted by flowing nitrogen (N_2) gas to evacuate excess reactants and products. The pump-down is required to bring the reaction chamber down to the base pressure of 30 mTorr.

Most of the ALD experiments on FiberForm employed a timing sequence of 12–10–15–12–10–15. The timing sequence was changed to 3–5–15–3–5–15 for smaller FiberForm samples. The TMA and H_2O reactants were dosed at 300 mTorr. N_2 flowed at 200 SCCM during the purge steps. This N_2 gas flow initially spiked to a pressure of 3 Torr before reducing to a steady 1 Torr in the reactor.

Nucleation difficulties are observed for Al_2O_3 ALD on carbon nanotubes. The sp^2 carbon surfaces are relatively chemically inert to the TMA and H_2O reactants.[37–39] The same nucleation difficulties were observed during Al_2O_3 ALD on the carbon fibers in the FiberForm. Consequently, a nucleation layer was formed on the FiberForm prior to conducting TMA and H_2O reactant exposures. The carbon surface can be functionalized for Al_2O_3 ALD by exposure to sequential exposures of nitrogen dioxide (NO_2) and TMA. NO_2 adsorbs to the carbon surface and creates reaction sites for TMA. This adsorbed NO_2 adlayer forms an adhesion layer that facilitates the nucleation of Al_2O_3 ALD.[38,39]

These experiments employed a functionalization process consisting of ten cycles of NO_2 and TMA at similar deposition parameters as the Al_2O_3 ALD process. NO_2 exposures were conducted for 10 s at a pressure of 500 mTorr. TMA exposures were performed for 10 s at a pressure of 300 mTorr. This sequence of ten cycles is believed to form an adhesion layer that is one layer thick because NO_2 does not react with the methyl-terminated surface after TMA exposures.[38,39]

B. Gravimetric analysis of Al_2O_3 ALD on the FiberForm

Gravimetric analysis was used to monitor Al_2O_3 ALD on the FiberForm sample. This analysis involved weighing the FiberForm sample after Al_2O_3 ALD. The mass gain was then analyzed based on a gravimetric model. This gravimetric model allowed Al_2O_3 ALD to be nondestructively monitored on the FiberForm substrate.

The gravimetric model assumed that the mass, m, deposited by the Al_2O_3 ALD process can be determined by the following equation:

$$m = n \times \mathrm{GPC} \times SA \times \rho,$$

where n is the number of Al_2O_3 ALD cycles, GPC is the film growth per Al_2O_3 ALD cycle, SA is the surface area of the FiberForm sample, and ρ is the density of the deposited Al_2O_3 ALD material. The GPC for Al_2O_3 ALD determined via spectroscopic ellipsometry (J. A. Woolam Co., Inc., M-2000 UI EC-400) on a silicon witness wafer was 1.25 Å/cycle. The surface area was treated as constant during the Al_2O_3 ALD cycles because the change of surface area with the Al_2O_3 ALD film thickness is negligible when the carbon fiber radius is much larger than the Al_2O_3 ALD film thickness. For the carbon fibers with a radius of 5 μm, the error in surface area between the constant surface area and expanding surface area resulting from Al_2O_3 ALD is only 0.01% per nanometer of the Al_2O_3 ALD thickness.

The surface area of the FiberForm samples could be estimated by the specific surface area of the FiberForm that ranges between 0.2 and 0.4 m^2/g.[40] The density of the Al_2O_3 ALD films is 3.0 g/cm^3.[15] The specific surface area range gives upper and lower bounds for the amount of mass the FiberForm sample should gain per Al_2O_3 ALD cycle. The mass gain per Al_2O_3 ALD cycle for reactions that reach saturation over the entire surface area should be between 0.0075% and 0.015% of the initial FiberForm sample mass per cycle. The mass of the FiberForm samples was recorded before and after Al_2O_3 ALD with an electronic mass balance (RADWAG AS60/220 R2). The majority of deposition experiments used FiberForm samples with a starting mass of about 1.3 g. TGA required much smaller samples. The samples for TGA had initial masses between 40 and 80 mg.

C. SEM and EDS analysis of Al_2O_3 ALD on the FiberForm

Further characterization of Al_2O_3 ALD on the FiberForm was performed using scanning electron microscopy (SEM) and energy dispersive x-ray spectroscopy (EDS) (Hitachi SU3500). FiberForm samples were cross-sectioned with a razor blade to expose the interior. Axial cross sections were along the axis of the FiberForm cylinders. Radial cross sections were along the radius of the FiberForm cylinders. EDS was used to measure the atomic concentration of aluminum across the width of the sample at accelerating voltages of 10 and 30 keV.

D. Thermogravimetric analysis of Al_2O_3 on FiberForm

Thermogravimetric analysis was performed in air at atmospheric pressure using a Netzsch STA 449 F1 Thermal Analyzer

14 October 2024 23:23:38

Published under an exclusive license by the AVS

TGA. This TGA evaluated the effect of the Al_2O_3 ALD coating on the oxidation of the FiberForm. TGA determined the oxidation temperature and oxidation rate of virgin FiberForm and FiberForm substrates with Al_2O_3 ALD barrier coatings with thicknesses of 25, 50, 75, and 100 nm. The temperature program was set to increase to 1000 °C at a rate of 20 °C/min. The temperature then was held for 30 min at 1000 °C.

III. RESULTS AND DISCUSSION

A. Gravimetric analysis of Al_2O_3 ALD on FiberForm

Al_2O_3 ALD films were deposited on the FiberForm at 200 °C using 100–800 Al_2O_3 ALD cycles in 100 cycle increments following 10 cycles of NO_2/TMA. The timing sequence during Al_2O_3 ALD was 12–10–15–12–10–15. The reactant exposures were 300 mTorr. At an Al_2O_3 ALD growth rate of 1.25 Å/cycle, these Al_2O_3 ALD cycles produced samples with coating thicknesses that should range from 12.5 to 100 nm in 12.5 nm increments. Gravimetric analysis was used to measure the mass of the FiberForm samples versus the number of Al_2O_3 ALD cycles.

The percent mass gain versus the number of ALD cycles is plotted in Fig. 2 and compared with the upper and lower bounds from the gravimetric model. A linear relationship is observed between the percent mass gain and the number of cycles. The slope of this relationship yields a mass gain of 0.0135% per cycle. This mass gain % is equal to ~0.175 mg per cycle for samples with an initial mass of 1.3 g. This mass gain of 0.0135% per cycle is within the upper and lower bounds of the gravimetric model. The linear relationship and the percent mass gain suggest that the Al_2O_3 ALD reaction parameters were sufficient to fully saturate both TMA and H_2O reactions over the entire surface area during Al_2O_3 ALD.

In addition, this observed percent mass gain of 0.0135% per cycle can be used to calculate a more precise value for the specific surface area of the FiberForm. This calculation assumes that the TMA and H_2O reactions are both completing to saturation on the entire surface area of the FiberForm. This calculation yields a specific surface area of 0.36 m^2/g for the FiberForm sample.

Al_2O_3 ALD on the FiberForm also led to color changes in the coated FiberForm sample. Figure 3 compares pictures of axial cross sections of an uncoated sample of FiberForm and a FiberForm sample coated with 100 nm of Al_2O_3 ALD. The sample coated with 100 nm of Al_2O_3 ALD developed a blue tinge. Additionally, this coloring is uniform throughout the sample both on the exterior and in the interior revealed by the cross section. This uniform color indicates that the Al_2O_3 ALD film was deposited uniformly throughout the sample.

B. SEM and EDS analysis of Al_2O_3 ALD on FiberForm

Figure 4(a) shows an SEM image in the secondary electron mode of individual carbon fibers in the cross-sectioned surface of a FiberForm sample coated with 100 nm of Al_2O_3 ALD. Figure 4(b) displays the corresponding EDS map for the same SEM image in Fig. 4(a). In the EDS map, green denotes aluminum, yellow represents oxygen, and red designates carbon. There is a yellow-green coating of Al_2O_3 on the red carbon fibers that conforms to the geometry of the fiber. The exposed carbon that is observed in the image is likely the result of the film delaminating during the cross-sectioning process. Fragments of the delaminated Al_2O_3 ALD film can be discerned near the top left and bottom right of the images. Electron imaging of the exterior of the FiberForm samples does not exhibit the same delamination and exposed carbon that is clearly observed in the cross sections.

EDS scans were also recorded versus the number of Al_2O_3 ALD cycles at regular spatial intervals across the axial length of the

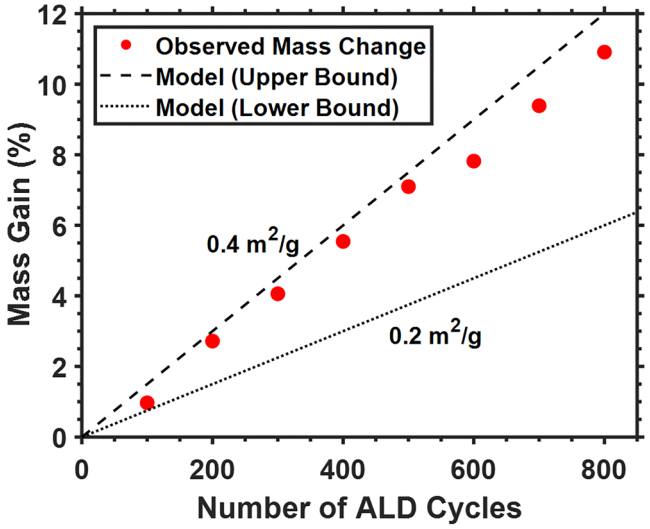


FIG. 2. Percent mass gain of FiberForm samples vs number of Al_2O_3 ALD cycles at 200 °C. Red solid circles indicate observed mass change. Dashed and dotted lines represent upper and lower bounds for the predicted percent mass gain based on specific surface areas for FiberForm of 0.2 and 0.4 m^2/g.

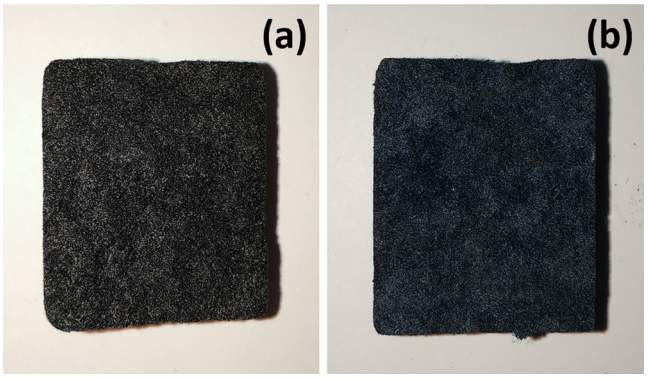


FIG. 3. Picture of an axial cross section of FiberForm (a) before and (b) after 800 Al_2O_3 ALD cycles at 200 °C. Al_2O_3 ALD-coated sample has blue tint resulting from optical interference effects in the Al_2O_3 film with a thickness of ~100 nm.

14 October 2024 23:23:38

Published under an exclusive license by the AVS

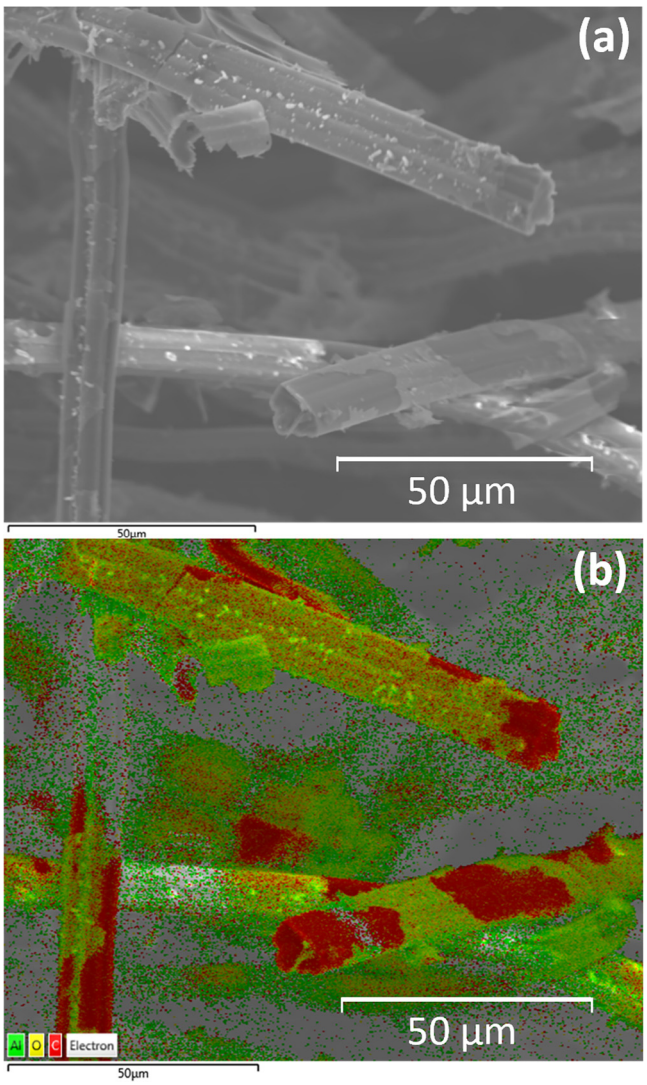


FIG. 4. (a) SEM image of carbon fibers in the interior of the FiberForm sample after coating with 800 Al_2O_3 ALD cycles at 200 °C. (b) EDS elemental map corresponding to Fig. 4(a). Green denotes aluminum, yellow represents oxygen, and red designates carbon.

FiberForm sample. These EDS scans measured the atomic concentration of aluminum. Al concentrations versus spatial position are plotted in Fig. 5 for the FiberForm samples coated with 200, 400, 600, and 800 cycles of Al_2O_3 ALD. Along the axis of the FiberForm sample, the Al concentration does not vary widely from one end to the center and to the opposite end. The aluminum concentration is also approximately proportional to the number of Al_2O_3 ALD cycles. These results demonstrate that the Al_2O_3 ALD coating is conformally covering the surface area of the entire FiberForm sample.

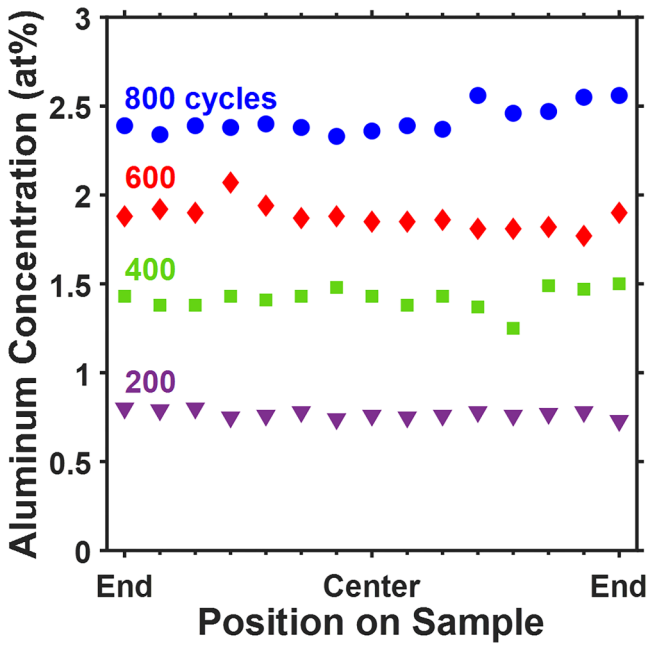


FIG. 5. Aluminum concentration vs position along the axis on axial cross sections of the FiberForm samples coated with varying numbers of Al_2O_3 ALD cycles at 200 °C. Aluminum concentration increases with the number of Al_2O_3 ALD cycles and is uniform across the sample.

C. Characterizing undersaturation reaction conditions

Confidence in the gravimetric model and characterization methods is strengthened by intentionally creating reaction conditions where Al_2O_3 ALD does not coat the entire surface area of the FiberForm sample. To probe these undersaturation conditions, four experiments on FiberForm were performed at reactant pressures of 100, 150, 250, and 300 mTorr using a timing sequence of 12–10–15–12–10–15 for 800 ALD cycles at 200 °C. The observed mass gain, predicted mass gain assuming saturation conditions, and film thickness on the witness wafer from these experiments are presented in Fig. 6.

The Al_2O_3 ALD thickness on the witness wafers decreases slightly as the dose pressure is decreased from 300 to 100 mTorr. The predicted mass gain was also calculated by the gravimetric model assuming saturation conditions with the more precise value for the specific surface area of the FiberForm. These predicted mass gains are proportional to the Al_2O_3 ALD thicknesses on the witness wafers. In contrast, the observed mass gain falls well below the mass gain predicted by the gravimetric model assuming saturation conditions at lower dose pressures. Al_2O_3 ALD is in undersaturation for dose pressures less than 250 mTorr.

Cross sections of the FiberForm were also inspected after reactant pressures of 100, 150, 250, and 300 mTorr using a timing sequence of 12–10–15–12–10–15 for 800 ALD cycles at 200 °C. Figure 7 compares the cross sections of these FiberForm samples for the various reaction conditions. For the images in Figs. 7(a)–7(d),

14 October 2024 23:23:38

Published under an exclusive license by the AVS

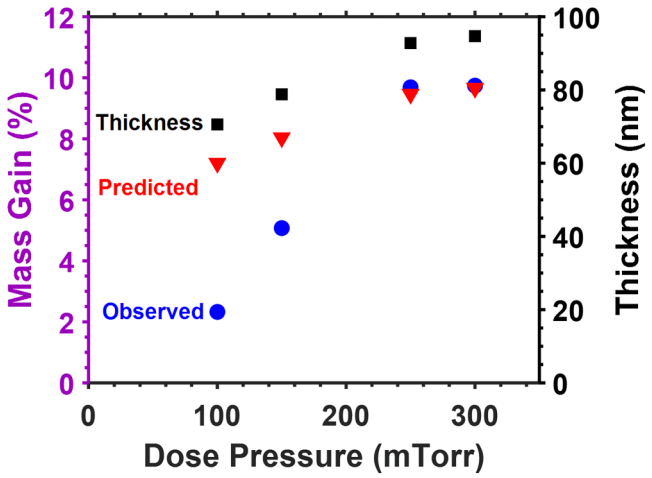


FIG. 6. Observed and predicted percent mass gain vs dose pressure for FiberForm samples after 800 cycles of Al_2O_3 ALD at 200 °C. Thicknesses of the Al_2O_3 ALD films on witness wafers are shown for comparison. Observed and predicted percent mass gains are equal for 250 and 300 mTorr dose pressures. Observed percent mass gains are much lower than the predictions for 100 and 150 mTorr dose pressures when the reactant exposures are in undersaturation.

the left side of each image is from the exterior surface. Axial cross sections in the middle of each image display the deposition penetration into the interior of the FiberForm sample. Radial cross sections on the right of each image show the radial progression of the deposition.

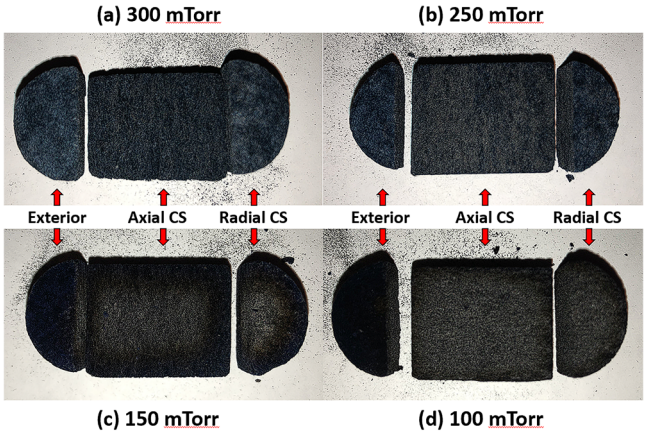


FIG. 7. Images of the exterior, axial cross section, and radial cross section of the FiberForm substrates after 800 cycles of Al_2O_3 ALD at 200 °C. Dose pressures were (a) 300, (b) 250, (c) 150, and (d) 100 mTorr. Substrates dosed with 300 or 250 mTorr exhibit the same blue tint as observed in Fig. 3. Substrates dosed with less pressure show coloration only at the edges of the cross sections.

For the samples dosed at 300 and 250 mTorr in Figs. 7(a) and 7(b), respectively, blue coloring is uniform throughout the exterior and cross sections similar to Fig. 3. For the sample dosed at 150 mTorr in Fig. 7(c), the portions of the image that show deposited material exhibit a blacker shade of blue. That coloring is only observed ~3 mm into the sample. The color returns to the gray observed in virgin FiberForm near the center of the FiberForm sample. There is even less penetration of the deposition into the sample dosed at 100 mTorr in Fig. 7(d). This optical examination indicates that Al_2O_3 ALD did not coat the FiberForm substrates uniformly at these lower pressures.

EDS analysis confirmed that the reaction conditions were in undersaturation at lower dose pressures. Figure 8 shows that the aluminum concentration is constant across the axial cross section of the FiberForm sample for Al_2O_3 ALD at larger dose pressures of 300 and 250 mTorr at 200 °C. Al_2O_3 ALD is in saturation at these higher dose pressures. In contrast, there is significant undersaturation at lower dose pressures of 150 and 100 mTorr.

Figure 8 indicates that the aluminum concentration is smaller at lower dose pressures of 150 and 100 mTorr at the ends of the FiberForm sample. The aluminum concentration also reduces versus distance along the axis of the FiberForm sample. The aluminum concentration approaches zero at the center of the FiberForm sample at these lower dose pressures. There are models for ALD in porous substrates that can be used to determine the type of ALD growth based on coverage profiles obtained during undersaturation conditions.[25,26,31,41] The aluminum concentration profiles at lower

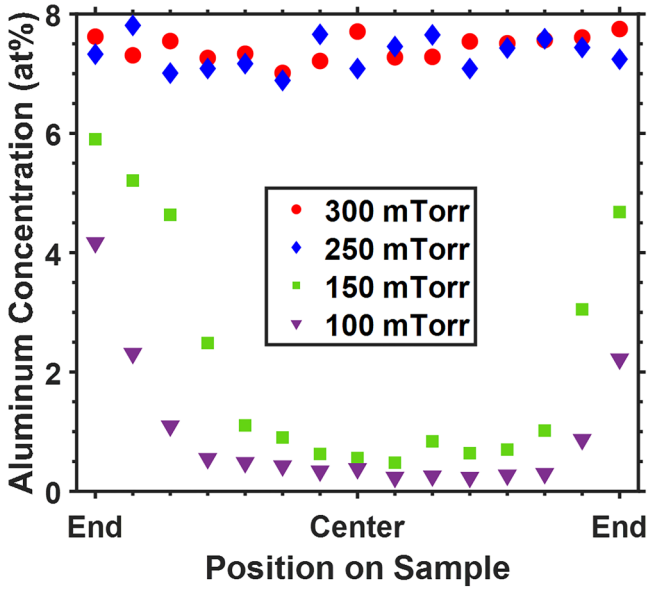


FIG. 8. EDS measurements of aluminum concentration vs relative position along the axis on axial cross sections for FiberForm substrates after 800 cycles of Al_2O_3 ALD for a range of dose pressures at 200 °C. A minimum in the aluminum concentration is present at the center of the substrates for reactant pressures of 100 and 150 mTorr. These dose pressures are in undersaturation.

14 October 2024 23:23:38

Published under an exclusive license by the AVS

dose pressures are consistent with diffusion-limited Al_2O_3 ALD.[25,26,31,41]

In diffusion-limited ALD, the coverage profiles decrease with distance into the porous substrate during undersaturation conditions.[25,26,31,41] The integrated ALD in the porous substrate also increases as $t^{1/2}$ where t is the exposure time.[26] In contrast, the reactants have time to penetrate the entire porous matrix during reaction-limited ALD. Under reaction-limited ALD conditions, the coverage profiles are constant with distance into the porous substrate and the integrated ALD in the porous substrate increases as t^1.[26,31] The aluminum concentration profiles in Fig. 8 for the dose pressures of 150 and 100 mTorr are expected for diffusion-limited Al_2O_3 ALD.[25,26,31,41] Testing for diffusion-limited ALD based on the integrated Al_2O_3 ALD amount in the porous FiberForm sample increasing as $t^{1/2}$ was not possible. The dose pressures in Fig. 8 were varied with a fixed exposure time.

Note that the measured aluminum concentrations are higher for the samples that have reached saturation in Fig. 8 compared with the saturation aluminum concentrations in Fig. 5. This difference results from the accelerating voltage of the electron beam. A lower accelerating voltage of 10 keV was employed for the measurements in Fig. 8. A larger acceleration voltage of 30 keV was used for the measurements in Fig. 5. The lower energy electrons have a smaller interaction volume and do not penetrate as far through the 100 nm Al_2O_3 ALD film. Consequently, these lower energy electrons detect less carbon and there is a higher signal ratio for aluminum to carbon.

Additional experiments were also conducted on witness wafers while decreasing the reactant exposure times from 12 to 1 s at a dose pressure of 300 mTorr. The GPC for Al_2O_3 ALD was constant for all of these reactant exposure times. This behavior indicates that Al_2O_3 ALD is in saturation on the witness wafers for this range of reactant exposure times.

D. Thermogravimetric analysis of Al_2O_3 ALD on FiberForm

TGA was employed to determine the effect of the Al_2O_3 ALD coating on the threshold temperature for oxidation and the oxidation rate of the FiberForm samples. Smaller FiberForm samples with masses ranging from 40 to 80 mg were used for the TGA studies. The smaller sample sizes were required because of the finite volume of the TGA sample probe. These samples were coated with 200, 400, 600, and 750 cycles of Al_2O_3 ALD at 200 °C. These Al_2O_3 ALD cycle numbers correspond to film thicknesses of 25, 50, 75, and 100 nm, respectively. The timing sequence during Al_2O_3 ALD for these smaller samples was 3–5–15–3–5–15. The reactant exposures were 300 mTorr.

TGA could detect the oxidation onset of the FiberForm samples. The TGA results highlighting the oxidation onset for an uncoated sample and the coated samples are presented in Fig. 9. The uncoated FiberForm sample begins losing mass from oxidation at about 500 °C. The FiberForm sample coated with 200 Al_2O_3 ALD cycles begins losing mass from oxidation at about 650 °C. The FiberForm samples coated with 400, 600, and 750 Al_2O_3 ALD cycles begin losing mass from oxidation at about 700 °C. The

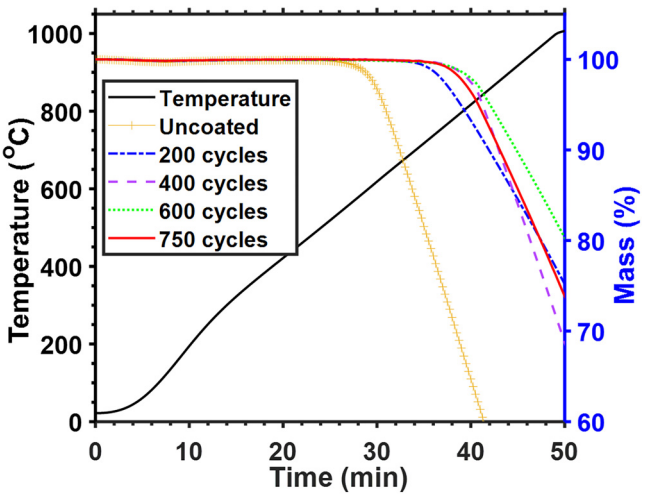


FIG. 9. TGA results showing mass percent and temperature vs time for uncoated FiberForm samples and FiberForm samples coated with varying numbers of Al_2O_3 ALD cycles at 200 °C. Black solid line shows the temperature program. Yellow hashed line represents uncoated FiberForm. FiberForm samples coated with 200, 400, 600, and 750 Al_2O_3 ALD cycles are represented by a blue dashed-dotted line, purple dashed line, green dotted line, and red solid line, respectively.

oxidation onset temperatures versus the number of Al_2O_3 ALD cycles are summarized in Fig. 10.

These oxidation onset temperatures versus the number of Al_2O_3 ALD cycles can be compared with earlier studies using Al_2O_3 ALD to limit the oxidation of carbon fibers. The earlier

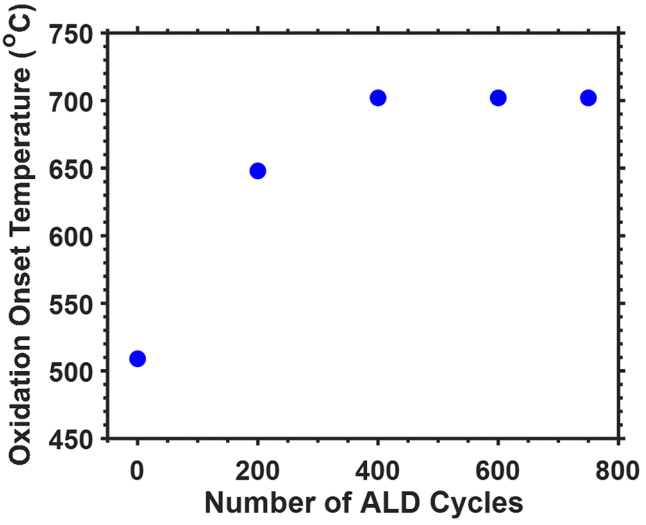


FIG. 10. Oxidation onset temperature for uncoated FiberForm and FiberForm coated with varying numbers of Al_2O_3 ALD cycles.

14 October 2024 23:23:38

Published under an exclusive license by the AVS

Al_2O_3 ALD studies showed that the oxidation onset temperature increased from 300 °C for an uncoated sample to 600 °C for a 30 nm coating of Al_2O_3 ALD.[11,24] A further increase in the oxidation onset temperature to 660 °C resulted from an Al_2O_3 ALD coating with a thickness of 120 nm.[11,24]

A possible mechanism for the oxidation of the ALD-coated FiberForm could be dependent on the cracking of the Al_2O_3 ALD coating. Al_2O_3 and the carbon fibers in the FiberForm have different coefficients of thermal expansion (CTE). The CTE of Al_2O_3 ALD has been reported as $2.1 \times 10^{-6}\,K^{-1}$.[42] The CTE of carbon fibers is anisotropic and behaves differently in the radial and longitudinal directions of the fibers. The radial CTE varies between 5 and $10 \times 10^{-6}\,K^{-1}$.[43] The longitudinal CTE varies between 1 and $2 \times 10^{-6}\,K^{-1}$ and has also been observed as slightly negative at lower temperatures.[43]

Because the radial CTE of carbon fiber is larger than the CTE of Al_2O_3 ALD, increasing the temperature of the ALD-coated FiberForm composite material above 200 °C will lead to tensile stress in the Al_2O_3 ALD film. Earlier studies have measured the critical stresses for cracking Al_2O_3 ALD films. Al_2O_3 ALD films will crack resulting from either tensile or compressive stresses.[44,45] The critical stresses for cracking from tensile or compressive stresses are also dependent on the thickness of the Al_2O_3 ALD film.[44] Thinner Al_2O_3 ALD films have higher critical stresses for cracking.[44] Film cracking will expose carbon of the ALD-coated FiberForm and lead to oxidation.

Another possible cause of oxidation is the crystallization of the Al_2O_3 ALD film. Al_2O_3 ALD films are usually deposited in an amorphous state.[46,47] Depending on the thickness of the films, Al_2O_3 ALD films start to crystallize to γ-Al_2O_3 at ~800 °C.[46,48] Thinner films generally require higher temperatures to crystallize than thicker films.[49,50] Crystallization could create defects and pinholes in the Al_2O_3 ALD coatings that could expose the underlying carbon to oxidation. However, oxidation is observed in ALD-coated FiberForm samples at temperatures lower than 800 °C. The crystallization of the Al_2O_3 ALD films is probably not the reason for the oxidation of the ALD-coated FiberForm samples.

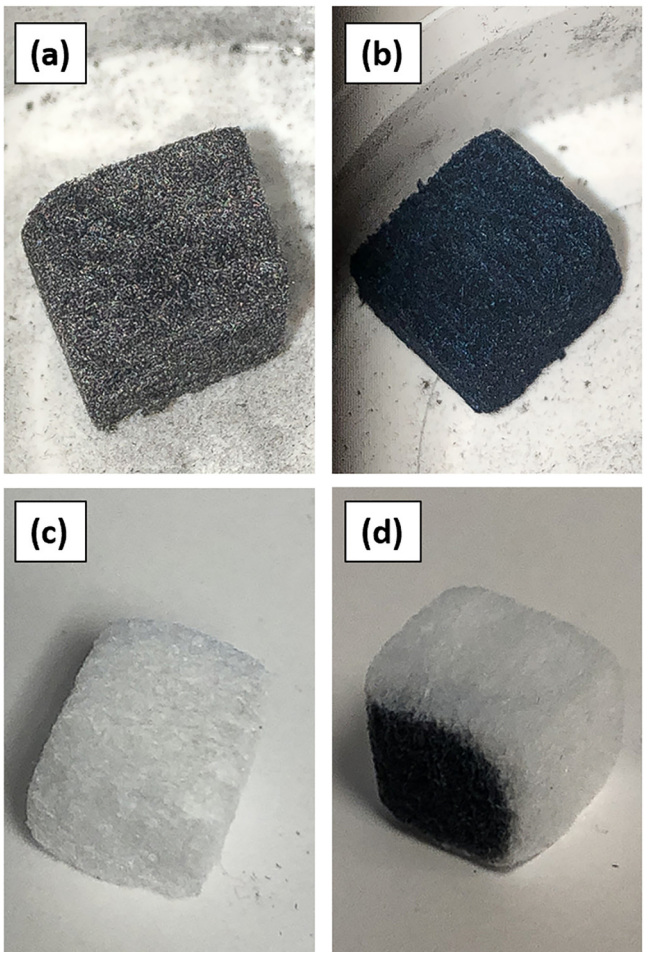


FIG. 11. Pictures of the FiberForm samples: (a) initial FiberForm sample; (b) FiberForm coated with 750 Al_2O_3 ALD cycles at 200 °C; (c) Al_2O_3 network left after TGA and complete oxidation of the FiberForm; and (d) Al_2O_3 network after TGA and incomplete oxidation of the FiberForm.

E. Al_2O_3 ALD coating remaining after FiberForm oxidation

Oxidation removes carbon from the Al_2O_3 ALD-coated FiberForm samples. The Al_2O_3 ALD coating remains behind and preserves the shape of the original FiberForm sample. Figure 11(a) displays a picture of an uncoated FiberForm sample. Figure 11(b) shows a photo of the Al_2O_3 ALD-coated FiberForm sample after 750 Al_2O_3 ALD cycles at 200 °C before TGA. Figure 11(c) displays a picture of the Al_2O_3 ALD-coated FiberForm sample after TGA. All the carbon has been removed by oxidation from the ALD-coated FiberForm sample in Fig. 11(c). The remaining white sample is the Al_2O_3 ALD coating that was deposited on the FiberForm sample using 750 Al_2O_3 ALD cycles. This FiberForm sample had a starting mass of ~55 mg.

Figure 11(d) displays a picture of another Al_2O_3 ALD-coated FiberForm sample after TGA. This sample was prepared using 600 Al_2O_3 ALD cycles and had a larger starting mass of ~75 mg. A small amount of carbon remains in this sample after TGA as shown in Fig. 11(d). The black color remaining on the sample in Fig. 11(d) was on the side of the FiberForm sample that was in contact with the bottom of the crucible during TGA. The larger sample would have required more time above the oxidation onset temperature to oxidize the entirety of carbon.

The unequal oxidation of carbon illustrated by the picture in Fig. 11(d) suggests that the oxidation of carbon in the Al_2O_3 ALD-coated FiberForm sample has a directionality. The white Al_2O_3 ALD "skeleton" on the outside of the FiberForm sample and the remaining black region that was at the bottom of the crucible are not consistent with uniform oxidation. Instead of oxidizing uniformly throughout the entire FiberForm sample, oxidation appears to occur from the outside to the inside of the Al_2O_3 ALD-coated FiberForm sample.

The leftover white Al_2O_3 ALD framework around the black region of the Al_2O_3 ALD-coated FiberForm in Fig. 11(d) suggests a

14 October 2024 23:23:38

Published under an exclusive license by the AVS

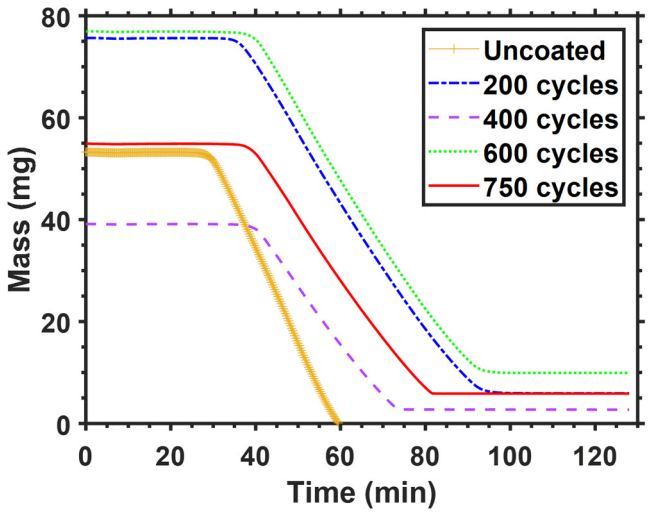


FIG. 12. Mass vs time during TGA of uncoated FiberForm and FiberForm coated with varying numbers of Al_2O_3 ALD cycles at 200 °C. Rate of mass loss vs time for the coated FiberForm samples is nearly equivalent.

mechanism for oxidation. The oxygen must travel through the hollowed-out Al_2O_3 framework and the produced carbon dioxide must travel out the opposite way to continue the oxidation. The flux of O_2 in and CO_2 out may establish a boundary layer that slowly moves to the interior of the coated FiberForm sample.

Figure 12 shows the mass of the various Al_2O_3 ALD-coated FiberForm samples versus time. The rate of oxidation is determined by the change of mass per change in time. The uncoated FiberForm sample has the highest oxidation rate. The rate of oxidation of the other Al_2O_3 ALD-coated FiberForm samples are very similar. The mass loss versus time is nearly constant and independent of the number of Al_2O_3 ALD cycles coating the FiberForm.

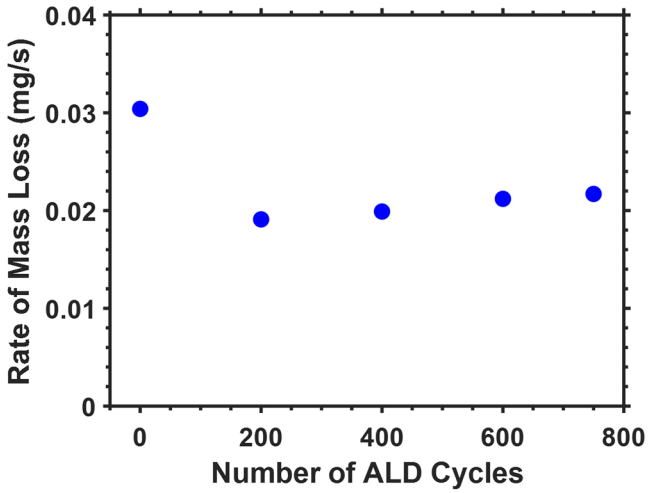


FIG. 13. Rate of mass loss for the various FiberForm samples shown in Fig. 12. Rate of mass loss is not dependent on the thickness of the Al_2O_3 ALD coatings.

The oxidation rates from the mass loss versus time in Fig. 12 are summarized in Fig. 13. The oxidation rate of the uncoated FiberForm sample is 50% faster higher than the Al_2O_3 ALD-coated FiberForm samples. In addition, the oxidation rate is remarkably similar for all Al_2O_3 ALD-coated FiberForm samples. This constant oxidation rate argues that carbon oxidation is dependent on the inward diffusion of O_2 into the coated FiberForm and the outward diffusion of CO_2 from the inside of the FiberForm. The opposing mass transport of these gases must generate a boundary layer that slowly moves into the FiberForm versus time.

IV. CONCLUSIONS

A porous matrix of carbon fibers (FiberForm) was coated with Al_2O_3 ALD using TMA and H_2O at 200 °C to improve oxidation resistance. Static reactant exposures with sufficient time and pressure were used to obtain uniform Al_2O_3 coatings on high porosity samples. The mass gain per cycle was used to monitor Al_2O_3 ALD versus the number of ALD cycles. Under conditions where the ALD reactions reached saturation during each reactant exposure, a gravimetric model was consistent with the mass gain per cycle.

SEM and EDS analysis were used to confirm the uniformity of the Al_2O_3 ALD coating on the FiberForm. When the ALD reactions reached saturation on the entire surface area, SEM, EDS, and the gravimetric model were all consistent with a uniform Al_2O_3 ALD coating on the porous carbon fiber network. In contrast, when the ALD reactions did not reach saturation throughout the FiberForm sample, the Al_2O_3 ALD coating on the FiberForm was not uniform. The Al_2O_3 coverage profile during these undersaturation conditions corresponded to diffusion-limited Al_2O_3 ALD.

TGA was employed to study the oxidation of the FiberForm and the Al_2O_3 ALD-coated FiberForm. TGA revealed enhanced oxidation resistance from a 50 nm thick Al_2O_3 coating deposited using 400 Al_2O_3 ALD cycles. The oxidation onset temperature increased by ~200 °C from 500 to 700 °C. The oxidation of the FiberForm removed carbon and left the Al_2O_3 ALD coating behind in a framework that preserved the original shape of the FiberForm sample. The Al_2O_3 ALD coating decreased the oxidation rate by ~30%. The oxidation rate of the FiberForm was also nearly independent of the thickness of the Al_2O_3 ALD coating. These results suggest that FiberForm oxidation is mass transport limited by O_2 diffusion into the FiberForm and CO_2 diffusion out of the FiberForm.

14 October 2024 23:23:38

ACKNOWLEDGMENTS

This research was funded by the NASA Ames Laboratory in Mountain View, California. The authors thank Brody K. Bessire of NASA Ames Laboratory for valuable discussions. The authors also acknowledge Alan Weimer and his research group at the Department of Chemical and Biological Engineering at the University of Colorado Boulder for TGA analysis.

Published under an exclusive license by the AVS

AUTHOR DECLARATIONS

Conflict of Interest

The authors have no conflicts to disclose.

Author Contributions

Jack T. Widmer: Conceptualization (supporting); Data curation (lead); Formal analysis (lead); Investigation (lead); Methodology (equal); Resources (lead); Validation (lead); Writing – original draft (lead); Writing – review & editing (supporting). **Steven M. George:** Conceptualization (lead); Funding acquisition (lead); Methodology (equal); Project administration (lead); Supervision (lead); Writing – original draft (supporting); Writing – review & editing (lead).

DATA AVAILABILITY

The data that support the findings of this study are available within the article.

REFERENCES

[1]D. D. Jayaseelan, Y. Xin, L. Vandeperre, P. Brown, and W. E. Lee, Compos. Part B **79**, 392 (2015).
[2]O. Uyanna and H. Najafi, Acta Astronaut **176**, 341 (2020).
[3]G. Pulci, J. Tirillò, F. Marra, F. Fossati, C. Bartuli, and T. Valente, Compos. Part A **41**, 1483 (2010).
[4]M. Rivier, J. Lachaud, and P. M. Congedo, Aerosp. Sci. Technol. **84**, 1059 (2019).
[5]J. Koo, W. Ho, M. Bruns, and O. Ezekoye, "A review of numerical and experimental characterization of thermal protection materials part ii: Properties characterization," in *48th AIAA/ASME/ASCE/AHS/ASC Structures, Structural Dynamics, and Materials Conference*, Honolulu, Hawaii, April 23-26, 2007 (American Institute of Aeronautics and Astronautics, Reston, VA, 2007). p. 2131.
[6]R. D. Mathieu, AIAA J. **2**, 1621 (1964).
[7]J. E. Sheehan, Carbon **27**, 709 (1989).
[8]D. W. McKee, Carbon **25**, 551 (1987).
[9]N. S. Jacobson and D. M. Curry, Carbon **44**, 1142 (2006).
[10]S. Chen, X. Qiu, B. Zhang, J. Xu, F. Zhong, B. Zhu, Y. Zhang, J. Ou-Yang, and X. Yang, J. Alloys Compd. **886**, 161143 (2021).
[11]A. K. Roy, W. Baumann, S. Schulze, M. Hietschold, T. Mäder, D. J. Nestler, B. Wielage, and W. A. Goedel, J. Am. Ceram. Soc. **94**, 2014 (2011).
[12]S. Latzel, R. Vaßen, and D. Stöver, J. Therm. Spray Technol. **14**, 268 (2005).
[13]E. L. Corral and R. E. Loehman, J. Am. Ceram. Soc. **91**, 1495 (2008).
[14]S. M. George, Chem. Rev. **110**, 111 (2010).
[15]M. D. Groner, F. H. Fabreguette, J. W. Elam, and S. M. George, Chem. Mater. **16**, 639 (2004).
[16]P. F. Carcia, R. S. McLean, M. D. Groner, A. A. Dameron, and S. M. George, J. Appl. Phys. **106**, 023533 (2009).
[17]P. F. Carcia, R. S. McLean, M. H. Reilly, M. D. Groner, and S. M. George, Appl. Phys. Lett. **89**, 031915 (2006).
[18]A. A. Dameron, S. D. Davidson, B. B. Burton, P. F. Carcia, R. S. McLean, and S. M. George, J. Phys. Chem. C **112**, 4573 (2008).
[19]M. D. Groner, S. M. George, R. S. McLean, and P. F. Carcia, Appl. Phys. Lett. **88**, 051907 (2006).
[20]T. Hirvikorpi, M. Vähä-Nissi, T. Mustonen, E. Iiskola, and M. Karppinen, Thin Solid Films **518**, 2654 (2010).
[21]T. O. Kääriäinen, P. Maydannik, D. C. Cameron, K. Lahtinen, P. Johansson, and J. Kuusipalo, Thin Solid Films **519**, 3146 (2011).
[22]R. Cooper, H. P. Upadhyaya, T. K. Minton, M. R. Berman, X. H. Du, and S. M. George, Thin Solid Films **516**, 4036 (2008).
[23]A. W. Weimer, J. Nanopart. Res. **21**, 9 (2019).
[24]A. K. Roy, S. Schulze, M. Hietschold, and W. A. Goedel, Carbon **50**, 761 (2012).
[25]V. Cremers, R. L. Puurunen, and J. Dendooven, Appl. Phys. Rev. **6**, 021302 (2019).
[26]J. W. Elam, D. Routkevitch, P. P. Mardilovich, and S. M. George, Chem. Mater. **15**, 3507 (2003).
[27]X. B. Meng, X. Q. Yang, and X. L. Sun, Adv. Mater. **24**, 3589 (2012).
[28]C. Detavernier, J. Dendooven, S. P. Sree, K. F. Ludwig, and J. A. Martens, Chem. Soc. Rev. **40**, 5242 (2011).
[29]C.-W. Kwon, J.-W. Son, J.-H. Lee, H.-M. Kim, H.-W. Lee, and K.-B. Kim, Adv. Funct. Mater. **21**, 1154 (2011).
[30]T. M. Onn, R. Kungas, P. Fornasiero, K. Huang, and R. J. Gorte, Inorganics **6**, 34 (2018).
[31]A. Yanguas-Gil and J. W. Elam, Chem. Vap. Deposition **18**, 46 (2012).
[32]T. Keuter, N. H. Menzler, G. Mauer, F. Vondahlen, R. Vaßen, and H. P. Buchkremer, J. Vac. Sci. Technol. A **33**, 01A (2015).
[33]C. Bae, H. Kim, E. Kim, H. G. Park, and H. Shin, Chem. Mater. **30**, 4748 (2018).
[34]J. W. Elam, M. D. Groner, and S. M. George, Rev. Sci. Instrum. **73**, 2981 (2002).
[35]A. W. Ott, J. W. Klaus, J. M. Johnson, and S. M. George, Thin Solid Films **292**, 135 (1997).
[36]A. C. Dillon, A. W. Ott, J. D. Way, and S. M. George, Surf. Sci. **322**, 230 (1995).
[37]D. B. Farmer and R. G. Gordon, Electrochem. Solid State Lett. **8**, G89 (2005).
[38]D. B. Farmer and R. G. Gordon, Nano Lett. **6**, 699 (2006).
[39]A. S. Cavanagh, C. A. Wilson, A. W. Weimer, and S. M. George, Nanotechnology **20**, 255602 (2009).
[40]Brody K. Bessire based on tomography values from NASA Ames Laboratory, personal communication (2022).
[41]W. Szmyt, C. Guerra-Nuñez, L. Huber, C. Dransfeld, and I. Utke, Chem. Mater. **34**, 203 (2022).
[42]J. T. Gaskins *et al.*, ECS J. Solid State Sci. Technol. **6**, N189 (2017).
[43]C. Pradere and C. Sauder, Carbon **46**, 1874 (2008).
[44]S. H. Jen, J. A. Bertrand, and S. M. George, J. Appl. Phys. **109**, 084305 (2011).
[45]S. H. Jen, S. M. George, R. McLean, and P. Carcia, ACS Appl. Mater. Interfaces **5**, 1165 (2013).
[46]J. A. Murdzek, A. Rajashekhar, R. S. Makala, and S. M. George, J. Vac. Sci. Technol. A **39**, 042602 (2021).
[47]S. K. Lee, S. Y. Park, Y. S. Yi, and J. Moon, J. Phys. Chem. C **114**, 13890 (2010).
[48]P. Nayar, A. Khanna, D. Kabiraj, S. R. Abhilash, B. D. Beake, Y. Losset, and B. Chen, Thin Solid Films **568**, 19 (2014).
[49]S. Jakschik, U. Schroeder, T. Hecht, M. Gutsche, H. Seidl, and J. W. Bartha, Thin Solid Films **425**, 216 (2003).
[50]L. Bloch, Y. Kauffmann, and B. Pokroy, Cryst. Growth Des. **14**, 3983 (2014).

14 October 2024 23:23:38

Published under an exclusive license by the AVS